Available online at www.sciencedirect.com
SCIENCE DIRECT
Acta Materialia 54 (2006) 2431–2439
Acta MATERIALIA
www.actamat-journals.com

A homogenization approach to diffusion simulations applied to $\alpha + \gamma$ Fe–Cr–Ni diffusion couples

Henrik Larsson [a,*], Anders Engström [b]

[a] Division of Physical Metallurgy, Department of Materials Science and Engineering, Brinellv. 23, The Royal Institute of Technology (KTH), SE-100 44 Stockholm, Sweden
[b] Thermo-Calc Software, Stockholm Technology Park, SE-113 47 Stockholm, Sweden

Received 11 November 2005; received in revised form 20 January 2006; accepted 22 January 2006
Available online 13 March 2006

Abstract

The diffusion of Fe, Cr and Ni in one dimension in and between one- and two-phase α/γ regions was simulated using independently assessed thermodynamic and kinetic data. Simulation results compare favourably with experimental results obtained previously by one of the present authors (A. Engström). For example, the formation of a γ layer between an α and a $\gamma + \alpha$ region is correctly predicted. Neither phase interfaces nor individual phases are explicitly considered; instead, locally averaged kinetic properties are used and locally minimized Gibbs energy is assumed.

Keywords: Simulation; Diffusion; Multiphase; Stainless steels

1. Introduction

Diffusion processes in multiphase mixtures are of great practical importance. A typical example is duplex stainless steels where the properties depend sensitively on the morphology and phase fractions of ferrite (α) and austenite (γ). There are essentially two different approaches to simulate these processes. The first approach is to try to solve the 'full problem' in two or three dimensions using, for example, the phase-field method. The drawback with this approach is the computational cost which is linked to the problem of obtaining sufficiently good statistics. The other approach is to simplify the problem to one dimension, which results in a computationally cheaper method at the cost of less microstructural information being obtained. Clearly, the two approaches are complementary. The purpose of the present work is to introduce a new model for one-dimensional simulations of multiphase diffusion problems.

A model for one-dimensional simulations of diffusion processes in multiphase systems was suggested by Bongartz et al. [1] and later extended by Engström et al. [2]. However, this model, although successfully applied to a large number of cases (see e.g. Ref. [3]), suffers from drawbacks. The first is that it relies on the existence of a single continuous matrix phase in which diffusion is assumed to occur. The second is that it is, in a sense, an inherently explicit method, which limits the size of time steps. Finally, Schwind [4] found that it does not conserve matter, although the error is generally quite small if the volume fraction of dispersed phases is small.

Another method is due to Morral et al. [5]. This also relies on a single continuous matrix phase. In the derivation it is assumed that the volume fraction of dispersed phases is small and the effect of dispersed phases on the long-range diffusion is neglected.

Lee [6] developed the method of Engström et al. [2] further, making it possible to treat cases where the matrix phase differs between different regions. However, in Lee's

* Corresponding author. Tel.: +46 8 7908308; fax: +46 8 207681.
E-mail addresses: Henrik@mse.kth.se (H. Larsson), Anders@thermocalc.se (A. Engström).

1359-6454/$30.00
doi:10.1016/j.actamat.2006.01.020

method it is necessary to solve a set of flux balance equations to obtain the fluxes over, and displacement of, interfaces separating different regions.

All of the methods mentioned above, as well as the method presented in this work, have in common that they assume that equilibrium is established locally with regards to, for example, phase fractions and phase compositions. However, the new method does not rely on a continuous matrix phase; rather it resembles a single-phase problem with the phase having average kinetic properties and chemical potentials corresponding, locally, to equilibrium. The same numerical procedure is applied across the whole interior of the domain, i.e. without considering interfaces. The full composition dependence of chemical potentials and mobilities is taken into account.

A method that is quite similar to the one presented here was developed by Engström [7], but it suffers from some numerical difficulties. It has never been publicized, although it is briefly mentioned in Ref. [3].

2. Simulation model

2.1. Basis of model

The basis of the simulation model used in this work has been described in detail earlier [8,9], but for the convenience of the reader it will be recapitulated. How this model is modified so as to be applicable to multiphase mixtures is described in the following section.

The treatment is limited to one dimension and the molar volume V_m is assumed to be constant. Only systems without interstitial species will be considered; with a few reasonable assumptions it is straightforward to include interstitials in the model. The diffusion problem is solved in the lattice-fixed frame of reference and it is assumed that the local fraction of vacancies always corresponds to equilibrium and that no pores are formed as a result of vacancy annihilation.

With the present assumptions the volume- and number-fixed frames of references are identical. The number-fixed frame of reference is defined by the condition that the number of atoms on each side of a reference plane stays constant. The velocity of an inert marker, fixed to the lattice, relative to the number-fixed frame of reference is given by

$$v = -V_m \sum J_k, \tag{1}$$

where J_k is the flux of species k in the lattice-fixed frame of reference. This is generalized by introducing a time-dependent spatial coordinate $\tilde{z}$ defined by

$$\frac{d\tilde{z}}{dt} = v = -V_m \sum J_k, \tag{2}$$

with the initial condition $\tilde{z}(t=0) = z$, where z is the ordinary time-independent spatial coordinate. For any given time there thus exists a 1–1 mapping of $\tilde{z}$ into z. In other words, the fluxes are calculated in a lattice-fixed frame of reference but by simultaneously solving Eq. (2) the resulting concentration fields are mapped to a number-fixed frame of reference.

From absolute reaction rate theory arguments the following flux expression in the lattice-fixed frame of reference was obtained [9]

$$J_k = -\frac{M_k RT}{V_m \Delta\tilde{z}} \sqrt{x_k^1 x_k^2}\, 2\sinh\left(\frac{\Delta\mu_k}{2RT}\right), \tag{3}$$

where x_k^1 and x_k^2 denote the mole fraction of species k on plane/source 1 and 2, respectively, M_k is the mobility of species k, $\Delta\tilde{z}$ is the distance between the centres of the two planes/sources and $\Delta\mu_k$ is the difference in chemical potential.

2.2. Homogenization modification of previously derived model

The model as described above is applicable to one-phase problems and to moving phase boundary problems, but it cannot be applied to multiphase mixtures. However, by simply assuming locally minimized Gibbs energy and locally averaged kinetic properties it can be applied to a range of different problems, including multiphase mixtures. Locally minimized Gibbs energy means that the local phase fractions, phase compositions, etc., correspond to the equilibrium values given by the local composition. This is often, but certainly not always, a good approximation if the local microstructural length scale is small compared to the global, or long-range, diffusion distance. How to choose locally averaged kinetic properties is a more complicated problem and is discussed in the next section. However, to emphasize these modifications Eq. (3) is rewritten with μ_k replaced with $\mu_k^{\text{l.eq.}}$ and M_k replaced with M_k^{eff}. Superscript l.eq. means local equilibrium signifying that the local chemical potential is obtained from the local minimum in Gibbs energy and eff stands for local effective mobility:

$$J_k = -\frac{M_k^{\text{eff}} RT}{V_m \Delta\tilde{z}} \sqrt{x_k^1 x_k^2}\, 2\sinh\left(\frac{\Delta\mu_k^{\text{l.eq.}}}{2RT}\right), \tag{4}$$

x_k^1 and x_k^2 denote the local overall mole fraction regardless of the number of phases present locally.

2.3. Calculating the 'effective' mobility M_k^{eff}

Diffusive transport belongs to a general class of transport properties, which among others include thermal conduction, electrical conduction, dielectric displacement and magnetic induction. The common mathematical structure of these phenomena is a linear relation between vector fields:

$$J_k = -\sum L_{ki} X_i, \tag{5}$$

where J_k here stands for any type of flux, e.g. diffusion of species, heat or electric charge, and X_i is a force, e.g. gradient of chemical potential, temperature or electric potential.

The L_{ki} are the appropriate materials descriptors, e.g. diffusivity, thermal conductivity or electrical conductivity.

For these phenomena a variety of combining rules exist for determining 'effective' transport properties in multiphase mixtures, from the transport properties in the individual phases, the fraction of phases and sometimes also from their geometrical distribution [10–14]. In addition, the common mathematical structure of these constitutive relationships suggests that combining rules developed for one set of transport properties apply also to the others. It is thus tempting to consult this literature in order to find suitable combining rules, which will allow the M_k^{eff} in Eq. (4) to be calculated from the M_k of the individual phases.

Combining rules, as for example in Refs. [10–14], are usually derived for fluxes which are described by a diagonal L matrix. In that case the material descriptors reduce to a scalar in an isotropic multiphase alloy. If correlation effects are ignored, then the mobility matrix M also reduces to a diagonal matrix in the isotropic case.

It is possible and many times useful to derive bounds. The simplest examples are the Wiener bounds [15] derived only on the basis of information about the fraction of the various phases under consideration. The lower bound comes from assuming a spatially uniform flux through each volume element, i.e.

$$M_k^{\text{eff}} = \left[\sum \frac{f^i}{M_k^i}\right]^{-1}, \tag{6}$$

where f^i is the volume fraction of phase i and M_k^i is the mobility of species k in phase i. The upper bound is defined from the assumption of a uniform force, in this case uniform chemical potential gradients:

$$M_k^{\text{eff}} = \sum f^i M_k^i. \tag{7}$$

These bounds are attained in fibrous and lamellar structures and are often referred to as a series and parallel model or the rule of mixtures and the inverse rule of mixtures.

As the Wiener bounds are rather far apart it is desirable to derive closer bounds by making further assumptions as made by Hashin and Shtrikman [16]. They used variational methods in order to obtain bounds for the effective magnetic permeability of multiphase composite materials assuming it to be, in a statistical sense, isotropic and homogeneous. If we apply their solution to a two-phase $\alpha + \gamma$ material, then we obtain the upper bound as

$$M_k^{\text{u}} = M_k^{\alpha} + \frac{f^{\gamma}}{\frac{1}{M_k^{\gamma} - M_k^{\alpha}} + \frac{f^{\alpha}}{3M_k^{\alpha}}}, \tag{8}$$

with $M_k^{\alpha} > M_k^{\gamma}$, which holds for Fe–Cr–Ni α/γ alloys. The geometry attained in this case is the 'composite sphere assemblage'; spheres of phase γ and radius r_{γ} are coated with shells of phase α and radius r_{α} such that r_{γ} and r_{α} enclose the relative amounts f^{γ} and f^{α} of the phases. All space is filled with composite spheres, which requires a distribution of radii including infinitesimally small values. If the spheres are interchanged so that spheres of phase α are coated by phase γ, then the effective mobility equals the lower Hashin–Shtrikman bound, i.e.

$$M_k^{\text{l}} = M_k^{\gamma} + \frac{f^{\alpha}}{\frac{1}{M_k^{\alpha} - M_k^{\gamma}} + \frac{f^{\gamma}}{3M_k^{\gamma}}}. \tag{9}$$

In the equations describing the bounds presented in Eqs. (6)–(9) it is assumed that the same phase is continuous throughout the whole interval even at very low fractions. In reality this is not likely to be the case. Imagine a dilute suspension of particles with high mobilities, dispersed in a matrix with very low mobilities. The 'effective' mobilities for this material will be very low, because it is controlled by the slow mobilities in the matrix. When increasing the volume fraction of the particles, the 'effective' mobilities will increase somewhat, but still be very low, until a critical volume fraction is reached where a continuous network of particles can be formed throughout the material. This critical concentration is known as the percolation threshold, and depends strongly on the phase geometries. Since the material behaves very differently above and below the percolation threshold, it is of great importance to be able to predict when it occurs. In general it is extremely difficult to predict the percolation threshold in real multiphase materials. For practical calculations one could use, for example, Eq. (8) below some predefined volume fraction of the low-mobility phase, and Eq. (9) above this fraction. In the current work calculations have been performed using both the upper and lower Hashin–Shtrikman bounds for purposes of comparison. Results are also presented from a simulation where a transition between the bounds was postulated to occur (see Section 4.4).

2.4. Numerical details

The system under consideration is divided into a number of initially equally sized slices; node points $\tilde{z}_0, \tilde{z}_1, \ldots$ correspond to the positions of the 'walls' between slices. $\Delta\tilde{z}$ in Eq. (4) is taken as the distance between centres of neighbouring slices. The chemical potentials and mobilities in each slice are calculated in each slice using the average composition of slices as input. For each time step, the coupled system of equations, given by Eqs. (2) and (4), yielding the fluxes between all neighbouring slices and the displacement of all node points is solved by an implicit procedure. The nature of the model and the implementation ensures that mass is conserved. Independently assessed thermodynamic and kinetic data used in simulations were obtained from the Thermo-Calc software [17].

3. Experimental

In order to validate the model the calculated results were compared against experimental work previously performed and published [18] by one of the authors. In this work five different multiphase diffusion couples according to Table 1 were fabricated from the Fe–Cr–Ni alloys presented in

Table 1
Diffusion couples

Couple	Temperature (°C)	Time (h)	Phase
k3–k7	1200	200	$\gamma/\gamma+\alpha$
k6–k7	1100	100	$\alpha/\gamma+\alpha$
k2–k5	1100	200	$\gamma/\alpha+\gamma$
k5–k7	1100	100	$\alpha+\gamma/\gamma+\alpha$

Table 2
Alloys (mass%)

Alloy	Cr	Ni
k2	12.5	4.9
k3	16.2	10.0
k5	24.3	6.9
k6	29.5	6.1
k7	40.0	29.4

Table 2. Details of the procedure of fabricating, annealing and analysing these diffusion couples will not be repeated here, as the interested reader can find this information in Ref. [18].

The alloy compositions and the temperature used during the diffusion anneals were selected in order to obtain different types of microstructures in the couples, and consequently different behaviours. All couples were encapsulated in quartz tubes under near vacuum and given individual diffusion anneals according to Table 1. In Table 1 the phases initially present on each side of the original diffusion interface are also indicated (the majority phase listed first).

Concentration profiles in the couples after diffusion annealing were determined by electron microprobe (EMP) measurements. Average concentrations in two-phase regions were determined by EMP measurements performed along lines at different distances from, but still parallel to, the original diffusion interface. Measurements were done both as one single line measurement, and by averaging several point measurements made along such a line.

4. Results from simulations and comparisons with experimental data

As an overview of the results obtained from simulations, diffusion paths plotted in the corresponding ternary phase diagrams for all diffusion couples are shown in Figs. 1 and 2. Micrographs reproduced from Ref. [18] showing the microstructures of the diffusion couples after annealing are shown in Figs. 3–6. In the micrographs, γ appears light and α dark.

4.1. Couple k3–k7

Results from simulations are presented in Figs. 7–9. This couple, which is of the type $\gamma/\gamma+\alpha$, exhibited no changes in the number of phase regions after the diffusion anneal. Experimentally it was observed that the two-phase region receded approximately 90 μm, whereas the simulation using the lower Hashin–Shtrikman bound showed a recession of about 50 μm. Here, as for couple k6–k7, use of the upper Hashin–Shtrikman bound gave wrongly a prediction of an advancing two-phase region. Consequently, also with regards to the composition profiles the lower bound gave the better prediction. In the micrograph it can also be seen that some Kirkendall porosity formed on the "k3 side" during the anneal. We conclude that diffusion in alloy k7 is below the percolation threshold for diffusion in α to dominate.

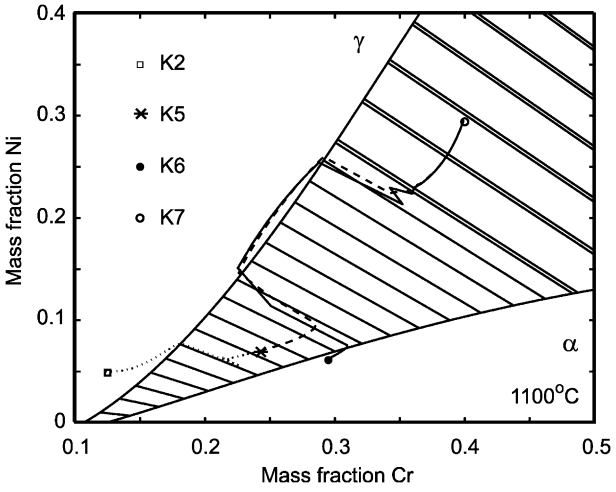

Fig. 1. Diffusion paths for couples k2–k5, k5–k7 and k6–k7. The phase diagram was calculated using Thermo-Calc [17].

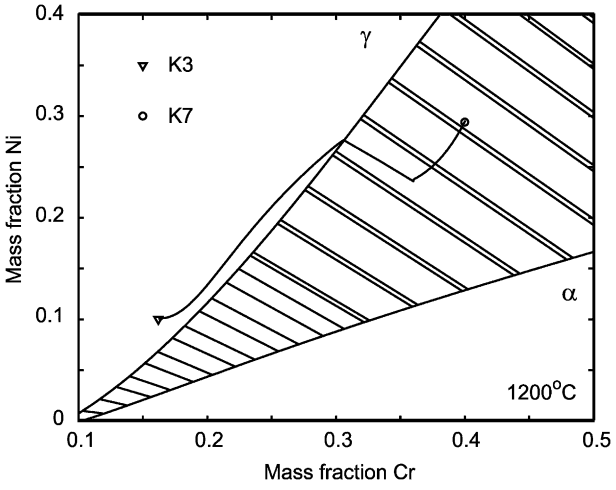

Fig. 2. Diffusion path for couples k3–k7. The phase diagram was calculated using Thermo-Calc [17].

4.2. Couple k6–k7

Results from simulations are presented in Figs. 10–12. The number of phase regions changed during the anneal from $[\alpha/\gamma+\alpha]$ to $[\alpha/\gamma/\gamma+\alpha]$, i.e. a single-phase γ layer formed. This layer was experimentally measured to be ~30 μm thick whereas the simulation using the lower bound predicted a thickness of ~20 μm. For the simulation using the upper bound, no single-phase γ layer was formed.

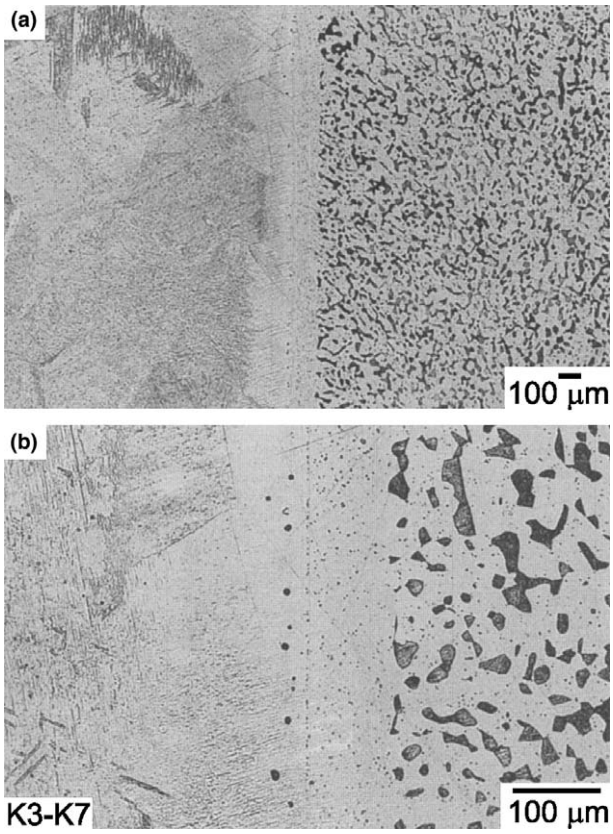

Fig. 3. Microstructure of diffusion couples k3–k7 after anneal. Reproduced from Ref. [18] with permission from Scandinavian Journal of Metallurgy and Blackwell Publishing.

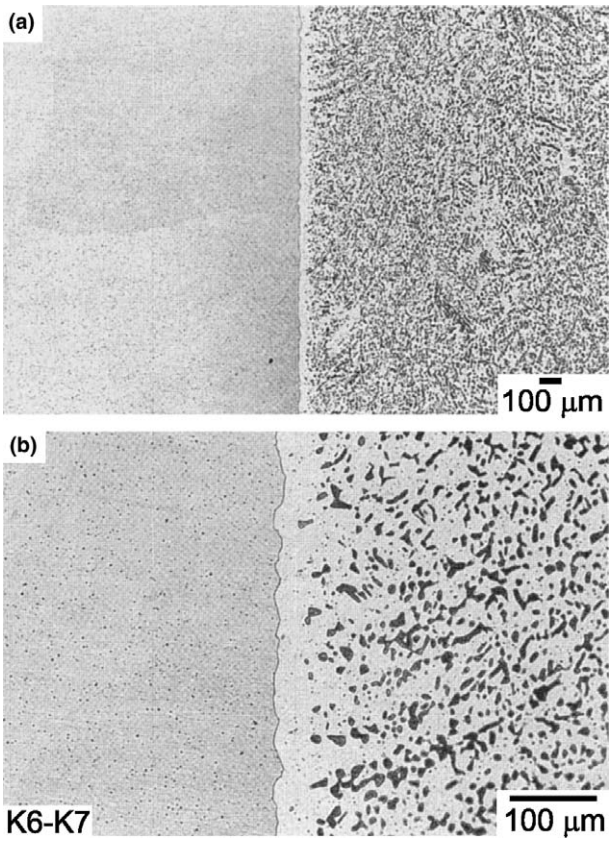

Fig. 4. Microstructure of diffusion couples k6–k7 after anneal. Reproduced from Ref. [18] with permission from Scandinavian Journal of Metallurgy and Blackwell Publishing.

4.3. Couple k2–k5

Results from simulations are presented in Figs. 13–15. For this couple no dramatic changes occurred. The $\alpha+\gamma$ region receded slightly, 10–20 μm. Also, the differences in simulation results between the two bounds were relatively small.

4.4. Couple k5–k7

Results from simulations are presented in Figs. 16–18. The number of phase regions changed during the anneal from $[\alpha+\gamma/\gamma+\alpha]$ to $[\alpha+\gamma/\gamma/\gamma+\alpha]$, i.e. a single-phase γ layer formed between the two-phase regions. This layer was experimentally measured to be ~50 μm thick whereas simulations using the lower and a mixed (see below) bound predicted a thickness of ~30 μm. Again, the simulation using the upper bound gave no prediction of single γ layer formation.

As discussed above in Section 2.3, a reasonable approximation would be to use the lower bound when the low-diffusivity phase has the highest volume fraction and vice versa. The dash–dot curves indicated as 'mixed' in Figs. 16–18 were obtained with this approximation in mind. The effective mobility was calculated ad hoc using a hyperbolic function to obtain a smooth transition between the bounds when the volume fraction of ferrite changes from about 0.4 to about 0.6, i.e.

$$M_k^{\mathrm{eff}} = M_k^{\mathrm{l}} + \frac{1}{2}\left[\tanh(30f^{\alpha}-15)+1\right]\left(M_k^{\mathrm{u}}-M_k^{\mathrm{l}}\right). \qquad (10)$$

As can be seen in the figures, the results obtained using this function are quite similar to those obtained using the lower bound.

5. Possible alterations of the model

The model as described above is primarily applicable to cases where the phases do not differ too much, e.g. when only solution phases are considered. However, consider for example the important case where carbides are dispersed in a ferritic or austenitic matrix; such a case has been simulated successfully using the model described in Ref. [2] (see Ref. [19]). It is clear from the geometric interpretation of the Hashin–Shtrikman bounds that the lower bound will yield far too small a flux; a sphere of matrix phase coated with a thin layer of carbide. At the same time the flux obtained from the upper bound will be too large. This is because the overall carbon content would enter the flux expression whereas in reality it is the transport in the matrix and the carbon solubility in the matrix that govern the long-range carbon diffusion, which is precisely the

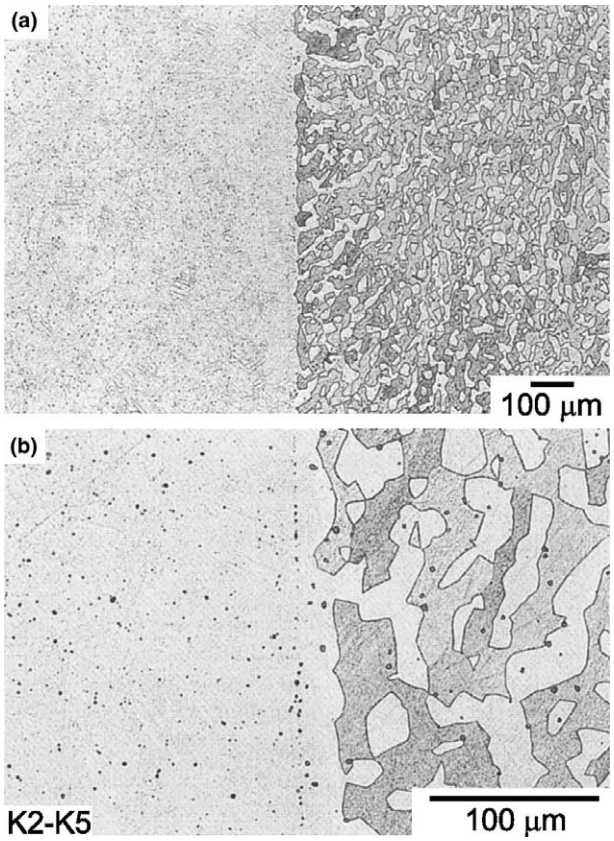

Fig. 5. Microstructure of diffusion couples k2–k5 after anneal. Reproduced from Ref. [18] with permission from Scandinavian Journal of Metallurgy and Blackwell Publishing.

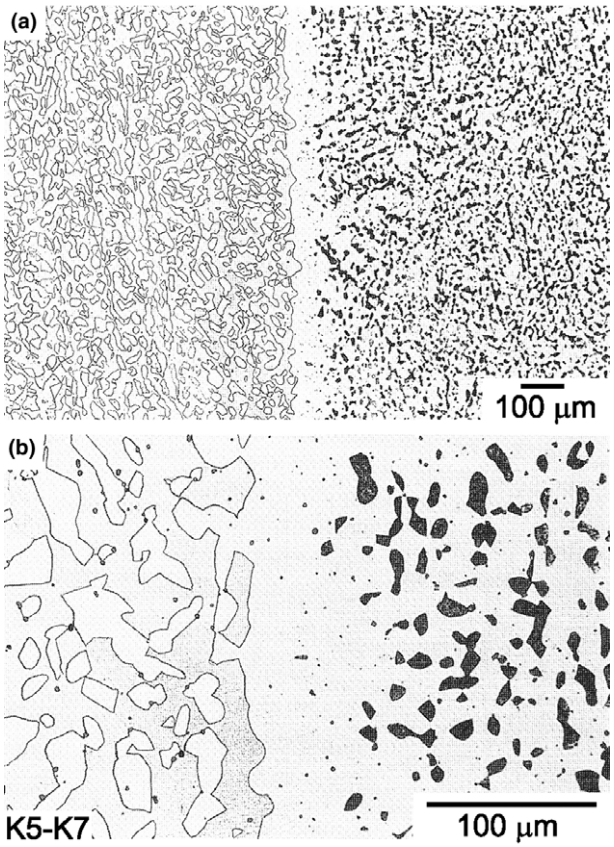

Fig. 6. Microstructure of diffusion couples k5–k7 after anneal. Reproduced from Ref. [18] with permission from Scandinavian Journal of Metallurgy and Blackwell Publishing.

assumption made in the model of Ref. [2]. Possible alterations of the model presented above will now be described. The basic assumption of local equilibrium will be retained, but two different ways of estimating the local kinetic properties will be suggested.

A first alteration is to view the content of species in the phases present as inherent parts of the kinetic properties. Taking this view it is the product $M_k^i x_k^i$, where i denotes the phase, that should be considered and the effective kinetic property to be evaluated is $[M_k x_k]^{\text{eff}}$. The flux expression would then be

$$J_k = -\frac{RT}{V_m \Delta\tilde{z}} \sqrt{[M_k x_k]^{\text{eff}1} [M_k x_k]^{\text{eff}2}}\, 2\sinh\left(\frac{\Delta\mu_k^{\text{l.eq.}}}{2RT}\right). \quad (11)$$

Another, more complex, possibility is to consider all combinations of pairwise phase interactions. This yields the following expression for the flux:

$$J_k = -\sum_i \sum_j f^{i1} f^{j2} \frac{M_k^{ij} RT}{V_m \Delta\tilde{z}} \sqrt{x_k^{i1} x_k^{j2}}\, 2\sinh\left(\frac{\Delta\mu_k^{\text{l.eq.}}}{2RT}\right), \quad (12)$$

where f^{i1} and f^{j2} are the fractions of phase i and j on sources 1 and 2, respectively. The mobilities M_k^{ij} can, as before, be approximated using the Hashin–Shtrikman bounds. Note that

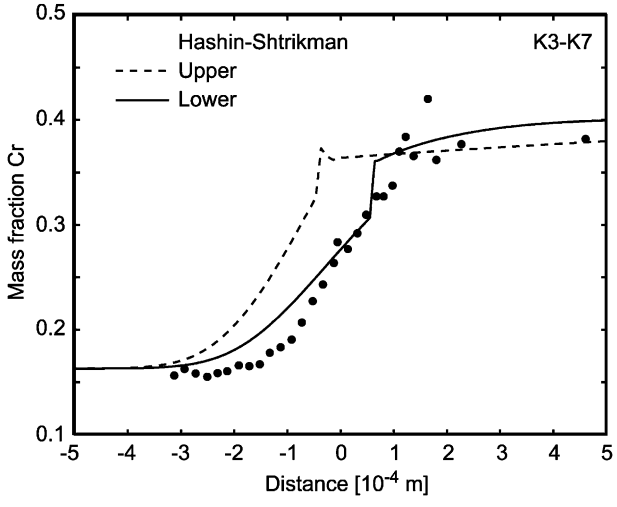

Fig. 7. Cr mole fraction profile for diffusion couples k3–k7.

$$\sum_i \sum_j f^i f^j = 1.$$

Eqs. (4), (11) and (12) are complementary to each other. Eq. (4) is the computationally cheapest. Eq. (11) is computationally slightly more expensive as all phase compositions must be evaluated.

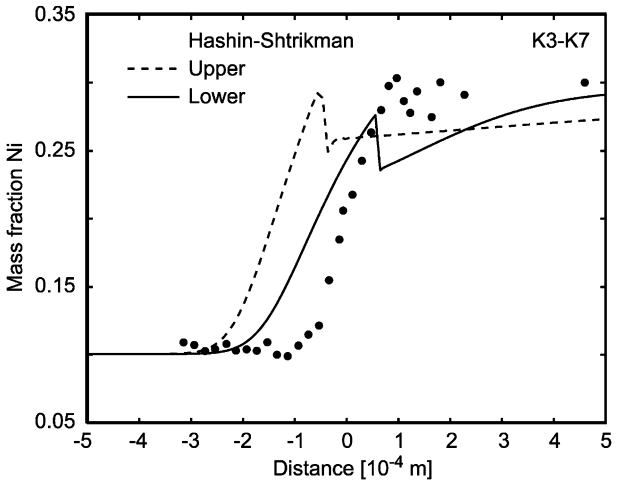

Fig. 8. Ni mole fraction profile for diffusion couples k3–k7.

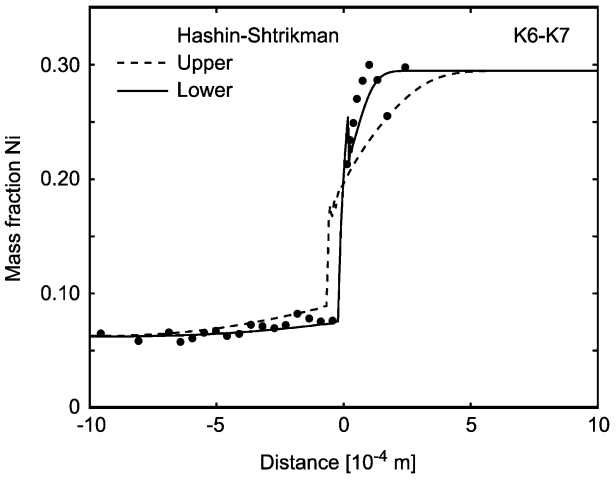

Fig. 11. Ni mole fraction profile for diffusion couples k6–k7.

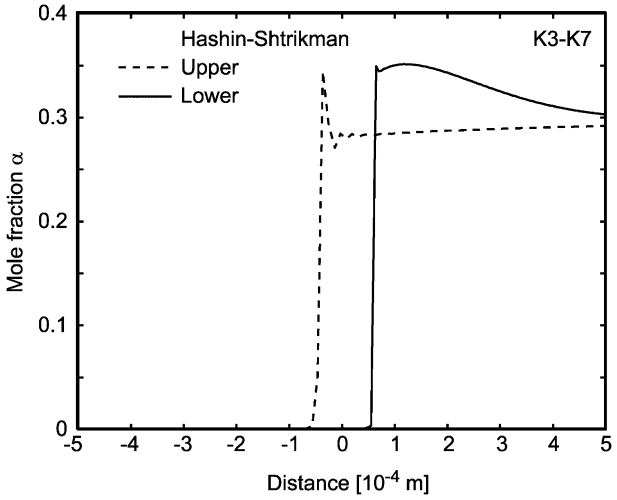

Fig. 9. α mole fraction profile for diffusion couples k3–k7.

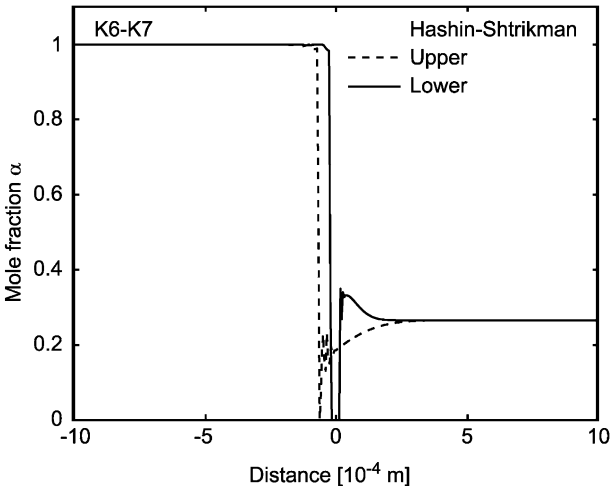

Fig. 12. α mole fraction profile for diffusion couples k6–k7.

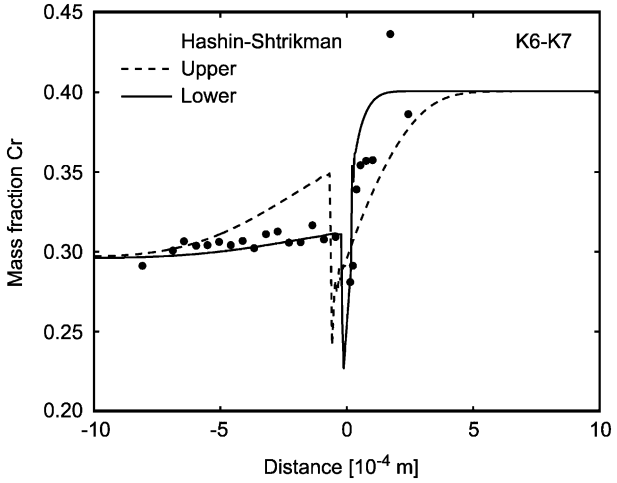

Fig. 10. Cr mole fraction profile for diffusion couples k6–k7.

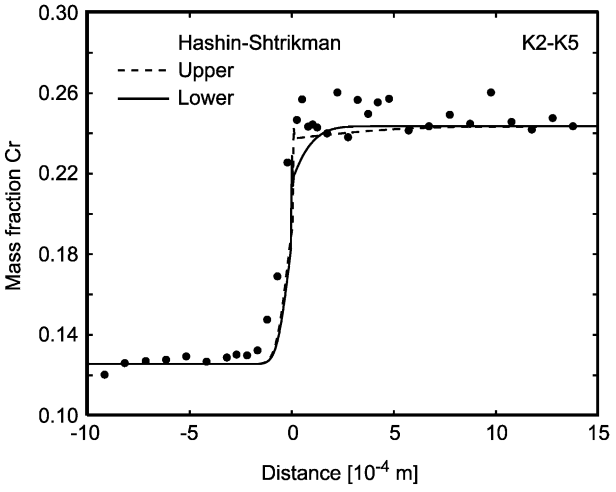

Fig. 13. Cr mole fraction profile for diffusion couples k2–k5.

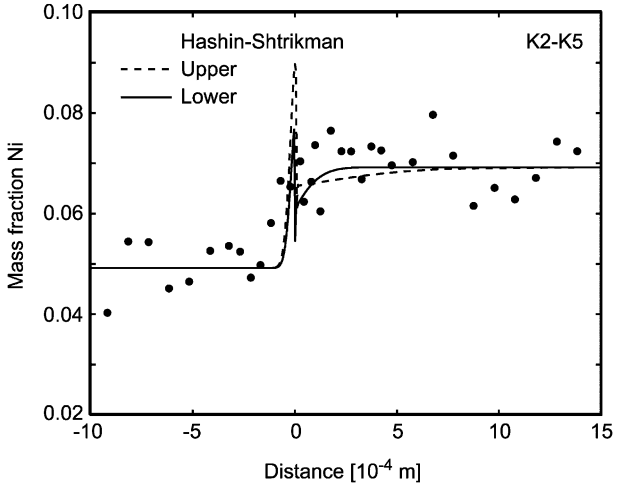

Fig. 14. Ni mole fraction profile for diffusion couples k2–k5.

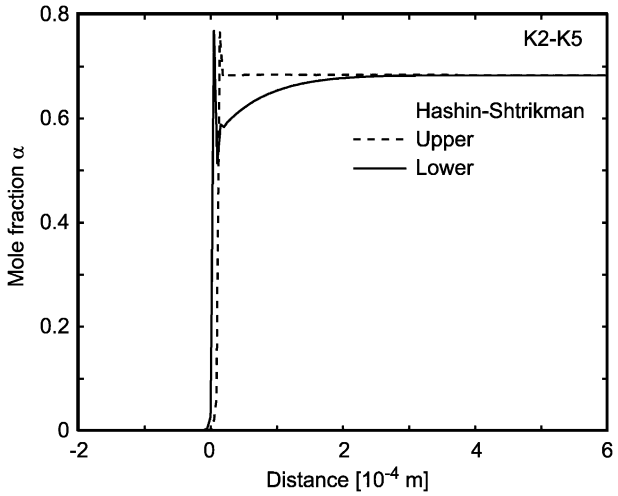

Fig. 15. α Mole fraction profile for diffusion couples k2–k5.

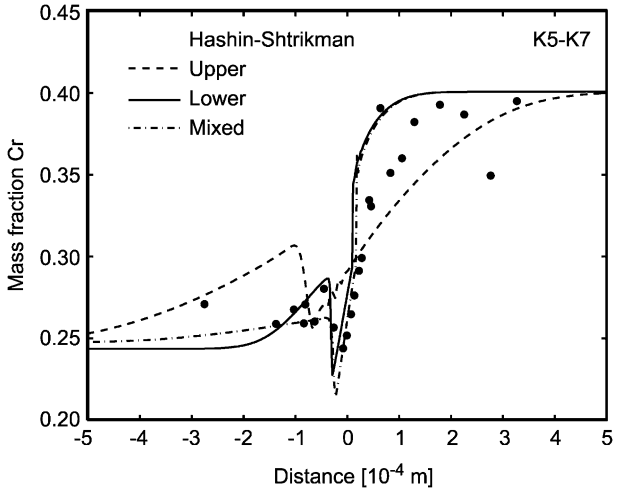

Fig. 16. Cr mole fraction profile for diffusion couples k5–k7.

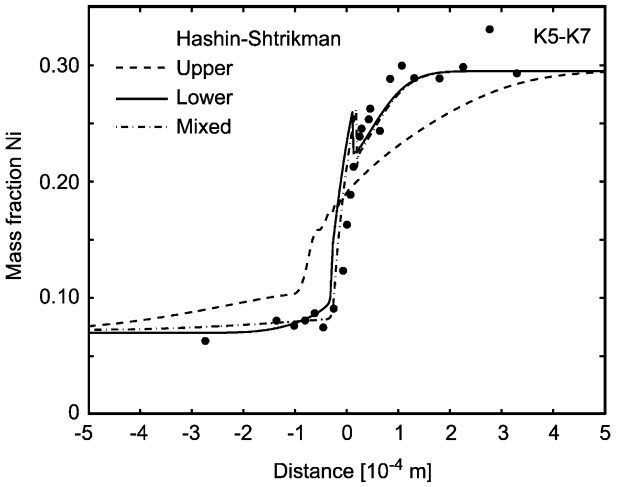

Fig. 17. Ni mole fraction profile for diffusion couples k5–k7.

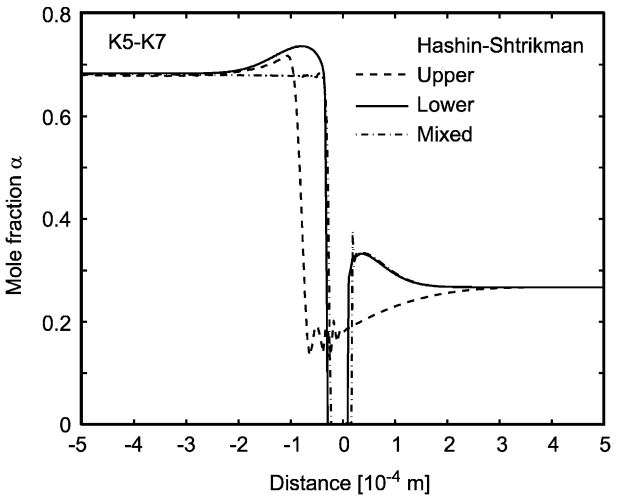

Fig. 18. α Mole fraction profile for diffusion couples k5–k7.

Eq. (12) is less dependent on which bound to use than the other two; an inherent assumption in Eq. (12) is that all phases with $f^i > 0$ are continuous.

6. Discussion

The simulation results obtained from the new model are highly encouraging. Using the lower Hashin–Shtrikman bound, predictions regarding the phase regions were qualitatively correct for all investigated cases. Regarding the composition profiles there was also a satisfactory quantitative agreement with experimental data. However, there is of course the question of predicting which bound to use. The choice of bound is of course only relevant for the two-phase regions. Of the two-phase alloys one (k7) has γ as the majority phase and for the other (k5) it is α. For diffusion in k7 the lower bound should thus be the better choice and vice versa. For the overall progress of diffusion in the couples it is the region with the lowest (effective) diffusivity that will control

the process. Only for couple k2–k5 would it therefore have been expected that the upper bound should have been the better choice. However, the heat treatment time for couple k2–k5 was insufficient to separate conclusively the bounds.

Numerically, the success of the model relies on the use of 'slices' and chemical potential gradients rather than dividing the domain into phase regions and working with concentration gradients; this ensures that singular gradients are entirely avoided. Some small 'fluctuations' can be seen in some of the curves. The nature of these is not fully understood. The numerical method used is unconditionally stable. Simulations using different number of node points and differing degrees of implicity gave roughly the same results.

The good agreement with experimental data confirms that the assumption of local equilibrium is sound for the system considered. The microstructural evolution is controlled by long-range diffusion.

A case for which the assumption is not expected to hold is where both dissolution and precipitation of stoichiometric low-diffusivity phases occur, such as for carbides and nitrides; this was the conclusion in a study of nitriding of tool steels [21] and a related example is the 'coring' phenomena during sintering of cemented carbides.

Acknowledgements

H.L. acknowledges funding from the Swedish Research Council. The Scandinavian Journal of Metallurgy and Blackwell Publishing are acknowledged for permission to reproduce Figs. 3–6 previously published in Ref. [18].

References

[1] Bongartz K, Lupton DF, Schuster H. Metall Trans A 1980;11A:1883.
[2] Engström A, Höglund L, Ågren J. Metall Mater Trans A 1994;25A:1127.
[3] Borgenstam A, Engström A, Höglund L, Ågren J. J Phase Eq 2000;21:269.
[4] Schwind M. Thesis, Stockholm: Royal Institute of Technology; 2001.
[5] Morral JE, Dupen BM, Law CC. Metall Trans A 1992;23A:2069.
[6] Lee B-J. Scripta Mater 1999;40:573.
[7] Engström A. Internal report, Trita-Mac 602. Stockholm: Department of Materials Science and Engineering, KTH; 1996.
[8] Strandlund H, Larsson H. Metall Mater Trans A; in press.
[9] Larsson H, Strandlund H, Hillert M. Acta Mater 2006;54:945.
[10] Bruggemann DAG. Ann Physik 1935;24:636.
[11] van Beek LKH. In: Birks JB, editor. Progress in dielectrics, vol. 7. London: Heywood; 1967. p. 69.
[12] Hale DK. J Mater Sci 1976;11:2105.
[13] Progelhof RC, Throne JL, Ruetsch RR. Polym Eng Sci 1976;16:615.
[14] Grimvall G. Thermophysical properties materials. Amsterdam: North-Holland; 1986.
[15] Wiener O. Abh Mat -Phy Kön Sächs Ges Wis 1912;32:509.
[16] Hashin Z, Shtrikman S. J Appl Phys 1962;33:3125.
[17] Sundman B, Jansson B, Andersson J-O. Calphad 1985;9:153.
[18] Engström A. Scand J Metall 1995;243:12.
[19] Helander T, Ågren J, Nilsson J-O. ISIJ Int 1997;37:1139.
[21] Larsson H, Ågren J. Metall Mater Trans A 2004;35A:2799.